

See discussions, stats, and author profiles for this publication at: <https://www.researchgate.net/publication/281274830>

Study on Structural, Mechanical, and Optical Properties of Al₂O₃ – TiO₂ Nanolaminates Prepared by Atomic Layer Deposition

ARTICLE in THE JOURNAL OF PHYSICAL CHEMISTRY C · AUGUST 2015

Impact Factor: 4.77 · DOI: 10.1021/acs.jpcc.5b06745

READS

83

8 AUTHORS, INCLUDING:



Igor Iatsunskyi

Adam Mickiewicz University

34 PUBLICATIONS 22 CITATIONS

[SEE PROFILE](#)



Roman Viter

Odessa National University

53 PUBLICATIONS 147 CITATIONS

[SEE PROFILE](#)



Ieva Baleviciute

Vilnius University

15 PUBLICATIONS 133 CITATIONS

[SEE PROFILE](#)



Karol Załęski

Adam Mickiewicz University

21 PUBLICATIONS 51 CITATIONS

[SEE PROFILE](#)

Study on Structural, Mechanical, and Optical Properties of Al_2O_3 – TiO_2 Nanolaminates Prepared by Atomic Layer Deposition

Igor Iatsunskyi,^{*,†} Emerson Coy,[†] Roman Viter,[§] Grzegorz Nowaczyk,[†] Mariusz Jancelewicz,[†] Ieva Baleviciute,^{||,‡} Karol Załęski,[†] and Stefan Jurga^{†,‡}

[†]NanoBioMedical Centre and [‡]Department of Macromolecular Physics, Adam Mickiewicz University, 85 Umultowska str., 61-614 Poznań, Poland

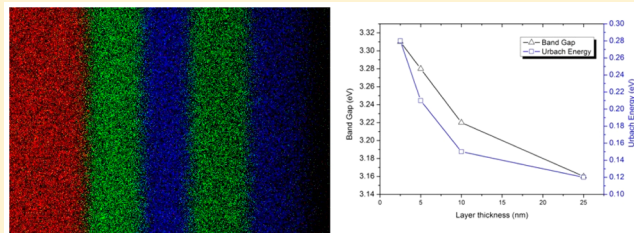
[§]Institute of Atomic Physics and Spectroscopy, University of Latvia, 19, Raina Blvd., LV 1586, Riga, Latvia

^{||}Department of Chemistry, Vilnius University, Naugarduko str. 24, LT-03225 Vilnius, Lithuania

[‡]Laboratory of BioNanoTechnology, Semiconductor Physics Institute, State Research Institute Center for Physical and Technological Sciences, A. Gostauto 11, LT-01108 Vilnius, Lithuania

Supporting Information

ABSTRACT: Structural, optical, and mechanical properties of Al_2O_3 / TiO_2 nanolaminates fabricated by atomic layer deposition (ALD) were investigated. We performed transmission electron microscopy (TEM), X-ray diffraction (XRD), X-ray reflectivity (XRR), energy dispersive X-ray spectroscopy (EDX), ellipsometry, UV-vis spectroscopy, photoluminescence (PL) spectroscopy, and nanoindentation to characterize the Al_2O_3 / TiO_2 nanolaminates. The main structural, optical, and mechanical parameters of Al_2O_3 / TiO_2 nanolaminates (thickness, grain size, refractive index, extinction coefficient, band gap, hardness, and Young's module) were calculated. It was established that with decreasing of the layer thickness, the value of band gap energy increases due to the quantum size effect related to the reduction of the nanograins size. On the other hand, the decreasing of nanograins size leads to generation of interface defects and, as a consequence, to the increasing of Urbach energy. It was also shown that there is an interdiffusion layer at the Al_2O_3 – TiO_2 interface, which plays a crucial role in explaining mechanical and optical properties of Al_2O_3 / TiO_2 nanolaminates. The correlation between structural, optical, and mechanical parameters was discussed.



1. INTRODUCTION

Nanolaminates are composite films formed by a number of alternating layers (e.g., metal oxides) of different materials each layer having its specific thicknesses on the nanometer scale. These multilayered structures demonstrate unique properties such as high dielectric constants^{1–3} and advanced mechanical,^{4–6} electrical,^{7–9} and optical^{10–12} properties. Nanolaminates of metal oxides (e.g., Al_2O_3 and TiO_2) with nanoscale thickness are known to have properties superior to that of a single film. Nanolaminates have better mechanical and tribological properties. Nanolaminates consisting of alternating Al_2O_3 and TiO_2 layers have been investigated for use as materials for advanced electronics/optoelectronics.^{13–17} Because of high thermostability and high optical transparency in the visible and ultraviolet spectra, these nanolaminates are especially useful for optical coatings.^{18,19}

Al_2O_3 / TiO_2 nanolaminates have been prepared by many techniques, such as chemical vapor deposition,²⁰ pulsed plasma-enhanced chemical vapor deposition,²¹ pulsed laser deposition,²² and atomic layer deposition (ALD).^{13–15,17–19} ALD is one of the most powerful methods for single layer and nanolaminates fabrication. Because of self-limiting reaction in the ALD process,

this method can be applied for planar samples,^{17–19} 3D patterned substrates,^{13–15} and porous materials (e.g., porous silicon).^{23–25}

Despite many publications devoted to the optical and electrical properties of Al_2O_3 / TiO_2 nanolaminates, further studies are still required. There is no information on how the morphology and chemical composition will affect optical and mechanical properties of fabricated nanolaminates. It is necessary to know the mechanical behavior of Al_2O_3 / TiO_2 nanolaminates because this finding could play a key role in the development of consistent theories of material behavior at the nanoscale. This is a challenging task, the solution of which requires a complex approach based on the use of different complementary experimental techniques. It is necessary to study the structure and tailoring the properties of the combined nanolaminates, and hence, the present work deals with structure, phase composition, and optical properties of the Al_2O_3 / TiO_2 nanolaminates and determines the relationship between the morphology, optical properties, and mechanical parameters as a function of nanolaminates layer thickness.

Received: July 14, 2015

Revised: August 20, 2015

In the present research, $\text{Al}_2\text{O}_3/\text{TiO}_2$ nanolaminates with different number of bilayers (BL) and layer thickness were deposited by ALD. Structural, optical, and mechanical parameters of $\text{Al}_2\text{O}_3/\text{TiO}_2$ nanolaminates (thickness, grain size, refractive index, extinction coefficient, band gap, hardness, and Young's module) were calculated, and the correlation between them was discussed.

2. EXPERIMENTAL SECTION

Synthesis of $\text{Al}_2\text{O}_3/\text{TiO}_2$ Nanolaminates by ALD. $\text{Al}_2\text{O}_3/\text{TiO}_2$ nanolaminates were deposited on p-doped Si (100) ($\rho < 0.005 \Omega \text{ cm}$) and glass substrates. Titanium tetrachloride (TiCl_4) and trimethylaluminum (TMA) ($(\text{CH}_3)_3\text{Al}$) were purchased from Sigma-Aldrich. Silicon and glass substrates were precleaned in acetone, ethanol, and deionized water. We used a Picosun ALD reactor for the fabrication of ultrathin $\text{Al}_2\text{O}_3/\text{TiO}_2$ nanolaminates. ALD was performed using sequential exposures of TMA/ TiCl_4 and H_2O separated by a purge of nitrogen (N_2) with a flow rate of 200 standard cubic centimeters per minute (sccm). The deposition using sequential exposures regime for Al_2O_3 and TiO_2 consisted of 0.6 s pulse of TMA/ TiCl_4 , 8 s of purge with N_2 followed by 0.6 s pulse of H_2O , and finally 8 s purge with N_2 . The deposition temperature was fixed to 200 °C. The growth rate was typically 0.45 Å per cycle for TiO_2 and 1 Å per cycle for Al_2O_3 . $\text{Al}_2\text{O}_3/\text{TiO}_2$ ultrathin nanolaminates with different number of cycles were deposited both on silicon and glass substrates by ALD (Table 1).

Table 1. ALD $\text{Al}_2\text{O}_3/\text{TiO}_2$ Nanolaminate Synthesis

samples	cycles of Al_2O_3	cycles of TiO_2	no. of bilayers	bilayer (BL) thickness (nm)
2 BL	250	500	2	50
5 BL	100	200	5	20
10 BL	50	100	10	10
20 BL	25	50	20	5

Material Characterization and Optical Measurements. Structural properties of $\text{Al}_2\text{O}_3/\text{TiO}_2$ nanolaminates were investigated by transmission electron microscopy (TEM) (JEOL ARM 200F high-resolution transmission electron microscope (200 kV) with an EDX analyzer). The cross sections and lamellae for TEM investigations were prepared by focused ion beam (FIB). The FIB milling was carried out with a JEOL JIB-4000. A carbon thin film was first deposited to protect the area of interest from surface damage during the FIB milling, and then the Ga^+ beam with different acceleration voltage (5–30 kV) was used to prepare lamellae. X-ray reflectometry (XRR) measurements were performed on X'pert³ MRD (XL) from PANalytical working with a $\text{Cu K}\alpha$ radiation source (wavelength of 1.54 Å) operating at 45 kV and 40 mA. The results were fitted using the X'Pert Reflectivity computer software package. The layer's density was not accurately measured and could not be reliably extracted from the model. Reasons are attributed to the intrinsic stress in the film, giving experimental artifacts in absorption and reflective index of the film, also to experimental problems in the sample mounting.

Optical properties of $\text{Al}_2\text{O}_3/\text{TiO}_2$ nanolaminates have been studied with UV-vis transmittance (UV-vis spectrophotometer lambda 950 UV/vis/NIR range 300–1100 nm, 1 nm step) and photoluminescence spectroscopy (FluoroSENS fluorometer). The spectroscopic ellipsometry method was used to obtain optical constants of Al_2O_3 and TiO_2 films. For this purpose

variable angle spectroscopic ellipsometer J.A. Woollam RC2 (USA) with dual rotating compensators operating in spectral range from 200 to 1700 nm was used. All ellipsometric measurements were carried out at four different angles of incident from 65° to 80° at step of 5°. Regression analysis constants was done using Complete EASE software from J.A. Woollam (USA).

Nanohardness and elastic modulus of the samples were measured by the nanoindentation (Hysitron TI 950 TribolIndenter) using a Berkovich diamond indenter at maximum load of 10 000 μN . Hardness and elastic modulus values were determined from the load–displacement curves by the Oliver–Pharr method.²⁶ Samples were measured a total of 15 times using the partial unloading function, with 50 increments, in order to allow depth profiling of the samples. The minimum penetration depth was set as 10 nm, in order to ensure the proper reproducibility of the calibrated Berkovich tip; moreover, long periods of drift correction were used in order to and avoid artifacts arising from the measurement. As methodology in the histogram analysis, any value with frequencies below 10 is ignored as experimental error.

3. RESULTS AND DISCUSSION

Morphology. In order to obtain information on the structure and the phase of the samples, X-ray analysis was carried out. Figure 1 shows the $2\theta-\theta$ scans of nanolaminates. The $2\theta-\theta$ scans show no evidence of superlattice structure. For thicker bilayer thickness, 2 BL sample, weak peaks at $2\theta = 25.44^\circ$ and 47.85° , corresponding to (101) and (200) reflections of anatase polymorph of TiO_2 (JCPDS-ICDD card No. 21-1272), have

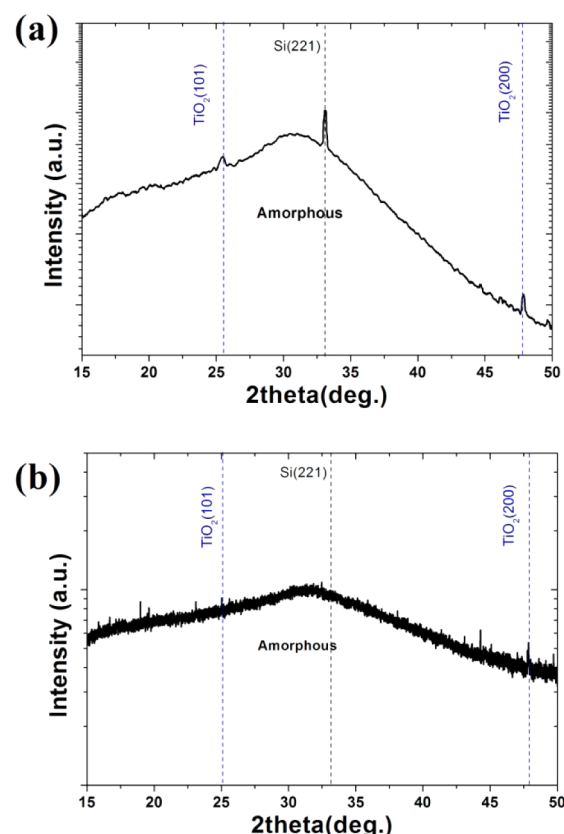


Figure 1. XRD patterns of $\text{Al}_2\text{O}_3/\text{TiO}_2$ nanolaminates: (a) 2 BL and (b) 5 BL.

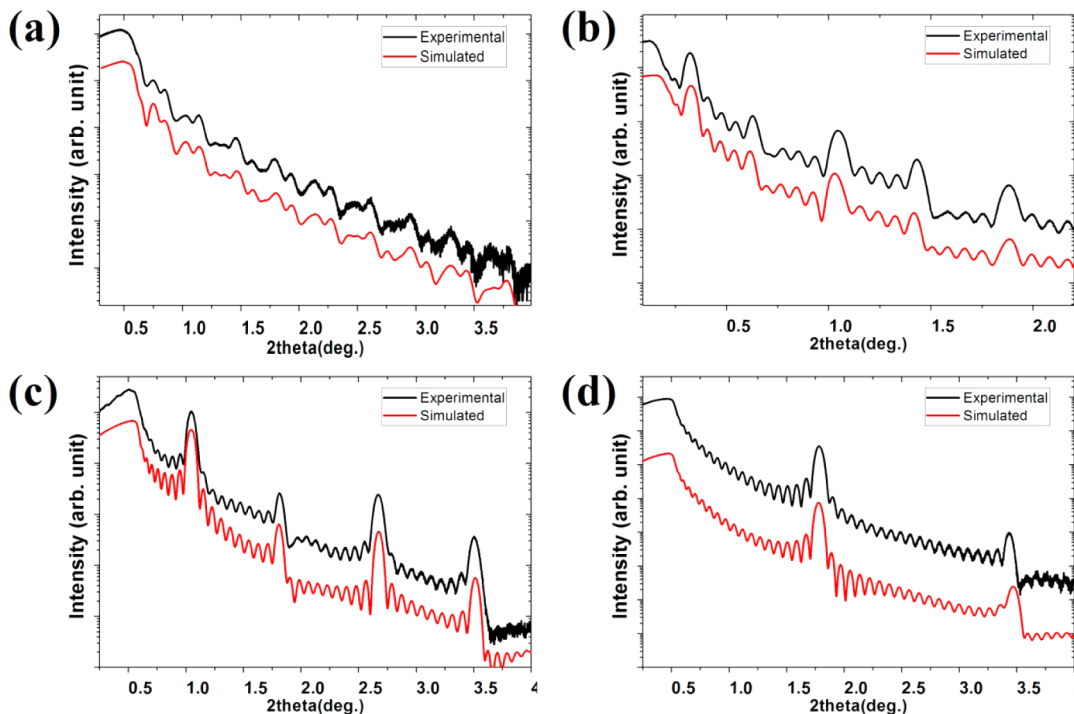


Figure 2. XRR measurement and simulation curves of $\text{Al}_2\text{O}_3/\text{TiO}_2$ nanolaminates with different number of bilayers: (a) 2 BL, (b) 5 BL, (c) 10 BL, and (d) 20 BL. Simulation curves are vertically offset for better clarity.

Table 2. Main Structural, Optical, and Mechanical Parameters of $\text{TiO}_2/\text{Al}_2\text{O}_3$ Nanolaminates^a

		samples			
		2 BL	5 BL	10 BL	20 BL
XRR	t_{TiO_2} [nm]	19.87 ± 0.4	8.99 ± 0.4	3.87 ± 0.35	1.44 ± 0.2
	$t_{\text{Al}_2\text{O}_3}$ [nm]	29.26 ± 0.4	9.61 ± 0.4	4.26 ± 0.4	1.62 ± 0.2
	t_{AlTiO} [nm]	1.67 ± 0.15	0.63 ± 0.15	0.93 ± 0.15	0.87 ± 0.12
	σ [nm]	0.53	0.45	0.27	0.31
TEM	t_{TiO_2} [nm]	23.4 ± 0.3	8.3 ± 0.3	4.2 ± 0.3	2.2 ± 0.15
	$t_{\text{Al}_2\text{O}_3}$ [nm]	25.3 ± 0.3	9.9 ± 0.2	6.1 ± 0.3	2.52 ± 0.15
optical parameters	E_g TiO_2 [eV]	3.16	3.22	3.28	3.31
	E_U [meV]	120	150	210	280
	n , TiO_2 (at 550 nm)	2.392 41	2.369 34	2.358 73	2.3504
	n , Al_2O_3 (at 550 nm)	1.6754	1.662 87	1.656 33	1.655 33
XRR	total layer thickness [nm]	103.3 ± 0.3	101.2 ± 0.1	101.8 ± 0.2	100.0 ± 0.2
	ellipsometry	103.7 ± 0.2	100.3 ± 0.2	100.4 ± 0.1	98.8 ± 0.2
mechanical parameters	E_1 [GPa]	140 ± 8	150 ± 2	137 ± 8	133 ± 8
	E_2 [GPa]	157 ± 5	166 ± 4	143 ± 8	152 ± 8
	H_1 [GPa]	8.7 ± 0.4	10.5 ± 0.7	9 ± 0.4	8.6 ± 0.5
	H_2 [GPa]	8.4 ± 0.4	9.03 ± 0.5	8.3 ± 0.5	8.0 ± 0.5
	H_3 [GPa]	7.9 ± 0.6			

^aParameters: t = layer thickness, σ = surface roughness, E_g = band gap energy, E_U = Urbach energy, n = refractive index, E = Young's modulus, H = hardness.

been observed (Figure 1a). The decrease of the BL thickness leads to the reduction of anatase peaks intensity (Figure 1b). A bulky background around 30° shows the presence of amorphous structures. Peaks related to Al_2O_3 were not observed. Therefore, the nanolaminates are essentially composed by amorphous Al_2O_3 and small TiO_2 crystalline regions.

Based on the XRD results, the mean size of TiO_2 nanocrystallite was determined from the full width at half-maximum (fwhm) of the XRD peaks using Scherrer's equation:²⁴

$$D = \frac{0.9\lambda}{\text{FWHM} \cos \theta} \quad (1)$$

where D and λ represent the nanocrystallite size and X-ray wavelength, respectively. The mean size of TiO_2 nanocrystallite for 2 BL sample was about 19.7 ± 1.2 nm and corresponded to the layer thickness.

XRR studies were performed on nanolaminates to study the formation of multilayers, individual layer thickness, BL thickness, interface roughness, and surface roughness. Measured and simulated XRR curves of $\text{Al}_2\text{O}_3/\text{TiO}_2$ nanolaminates with

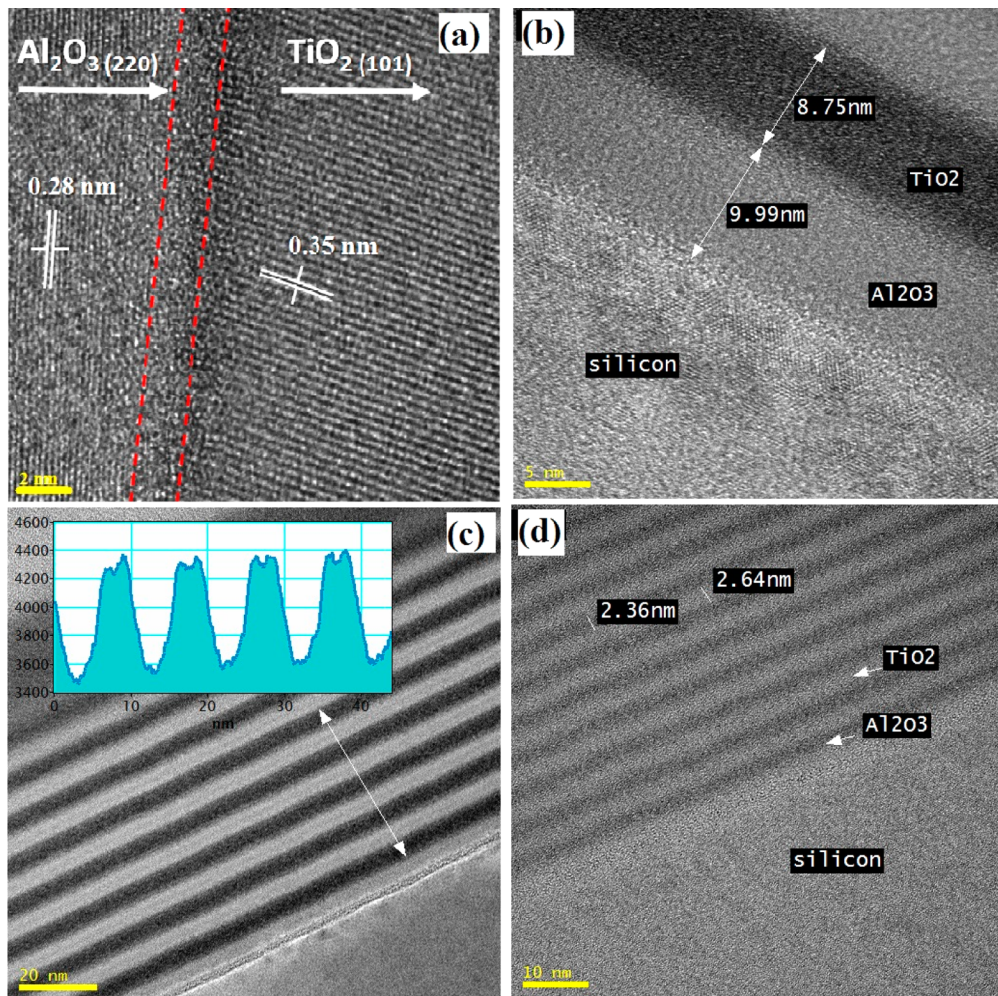


Figure 3. Cross-sectional view TEM image of $\text{Al}_2\text{O}_3/\text{TiO}_2$ nanolaminates with different number of bilayers: (a) 2 BL, (b) 5 BL, (c) 10 BL, and (d) 20 BL.

different number of BL are given in Figure 2, which shows how the XRR curves gradually change with decreasing BL thickness. The sharp maxima are characteristic of superlattice structures. Based on the fact that the fringe spacing is inversely proportional to film thickness, the layers thickness were determined.²⁷ In order to simulate XRR curves, we suggested that some interdiffusion layer (AlTiO) between Al_2O_3 and TiO_2 should exist. Calculations have shown that the thickness of this layer is about 1 nm for all samples (Table 2). We have assumed that this interdiffusion layer must affect the optical and mechanical properties of $\text{Al}_2\text{O}_3/\text{TiO}_2$ nanolaminates (shown later).

The small surface roughness values of the samples with 10 and 20 BL indicate that the TiO_2 films are amorphous, since crystalline films are known to have rough surfaces due to columnar growth.²⁸ The results of the XRR simulations are summarized in Table 2. The simulated parameters, like layer thickness and interdiffusion layer, are in good agreement with TEM results (shown later).

HRTEM was also used for structural characterization of the nanolaminates. Cross-sectional TEM images indicate that the $\text{Al}_2\text{O}_3/\text{TiO}_2$ nanolaminates are well prepared by ALD (Figure 3). From TEM images, it can be seen that the individual layers are of constant thickness and very reproducible (Supporting Information, Figure S1). The EDX mapping images showing the distribution of Al, Ti, and Si atoms also confirm nanolaminate

structure (Figure S2). The thicknesses of TiO_2 and Al_2O_3 layers are detected, which are consistent with the results measured from XRR. Crystallized TiO_2 shows clear lattice fringes, while a crystal structure could hardly be observed in Al_2O_3 layers. On the basis of XRD and TEM results, we can conclude that Al_2O_3 films are amorphous.

Figure 3a shows the interface between TiO_2 and Al_2O_3 layers for the sample with 2 BL. It could be clearly seen the interdiffusion layer (AlTiO) having approximate thickness 1.5 nm. This result is in a good agreement with XRR simulations. In Figure 3a we determined the fringe separation of 0.35 nm for anatase. Lattice fringes seen in HRTEM images reveal the TiO_2 crystal with (101) planes plane oriented perpendicular (or nearly perpendicular) to the film/substrate interfaces. It might be concluded that TiO_2 films grow on Al_2O_3 along the (101) direction. However, for samples with 5, 10, and 20 BL it was hard to reveal any crystalline structure (Figure 3b) due to the increasing influence of the interdiffusion layer and the progressive reduction of the layers thickness. Thus, the layers in the aforementioned samples were in amorphous or high polycrystalline phase. The results of the TEM analysis are summarized in Table 2.

Optical Measurements. The optical parameters were calculated for the nanolaminates deposited on glass and silicon substrates. Figure 4 shows the transmittance spectrum for the

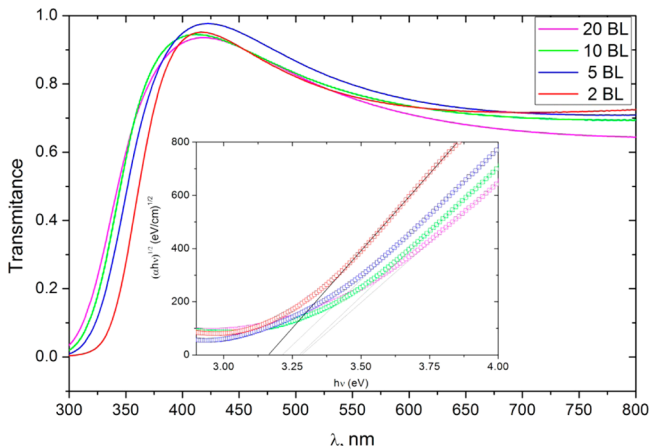


Figure 4. Transmittance spectra and band gap estimation (inset) of $\text{Al}_2\text{O}_3/\text{TiO}_2$ nanolaminates with different number of bilayers.

nanolaminates grown on the glass. The average transmittance over the entire visible wavelength range is more than 70%. Because of the strong absorption from fundamental band gap of TiO_2 , the absorption edge of the samples lies in the range of 350–400 nm. The blue-shift of absorption edge was observed with increase of BL numbers.

The average optical band gap value for TiO_2 was calculated according to the methodology described in ref 29. TiO_2 is known as a semiconductor with indirect optical transitions. Therefore, the optical density (OD) can be described by the equation²⁹

$$\text{OD} \sim \frac{(h\nu - E_g)^2}{h\nu} \quad (2)$$

where $h\nu$ and E_g are a photon energy and a band gap values, respectively. Plotting $(\text{OD} \cdot h\nu)^{1/2} \sim h\nu$, band gap values E_g were graphically calculated in the linear part of the absorption edge with respect to eq 2 (Figure 4 inset). The obtained values were 3.16, 3.22, 3.28, and 3.31 eV for 2, 5, 10, and 20 BL, respectively. Only for the samples with 2 and 5 BL (TiO_2 layer thickness 25 and 10 nm) does the band gap correspond to the bulk value of anatase (~3.2 eV). The sample with thinner layer showed higher values of the band gap, which could be related to the quantum confinement effect and/or doping of TiO_2 by Al during the ALD process.³⁰ Taking into account that the morphologies of TiO_2 films are significantly affected by the Al contents (Al content enhanced the nanocrystallinity of $\text{TiO}_2:\text{Al}$ film),³⁰ we suggest both the quantum confinement and the doping effects play significant roles. The obtained E_g values can also be affected by structural and point defects. In order to analyze the influence of defects on E_g we used methodology based on the Urbach law.^{31,32}

In amorphous and highly doped semiconductors the absorption coefficient/optical density depends on photon energy according to the Urbach law:^{31,32}

$$\text{OD} = \text{OD}_0 \exp\left(\frac{h\nu}{E_0}\right) \quad (3)$$

where E_0 is the Urbach energy interpreted as the width of the tails of localized states, corresponding to the amorphous state, in the forbidden gap of band gap tail. For the calculation of Urbach energy, $\ln(\text{OD})$ is plotted against $h\nu$. The calculated Urbach energy values are summarized in Table 2. The relation between the band gap, the Urbach energy, and the layer thickness is shown

in Figure 5. The Urbach energy decreases on going from the thinner to the thicker layer which means that from disorder to

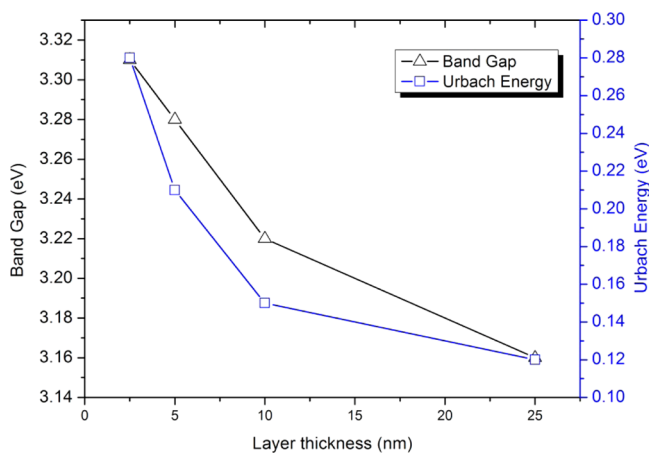


Figure 5. Band gap and Urbach energy estimation of $\text{Al}_2\text{O}_3/\text{TiO}_2$ nanolaminates with different layer thickness.

order, from amorphous to polycrystalline/crystalline structure. Choudhury et al. showed that the Urbach energy lying about 150 meV originates from oxygen vacancies or structural disordering at interface with different crystal phases.³¹ One can see that with decreasing of the layer thickness the value of band gap energy increases due to the quantum size effect related to the reduction of the nanograins size. On the other hand, the decreasing of nanograins size leads to generation of interface defects and, as a consequence, to the increasing of Urbach energy.

The spectroscopic ellipsometry method was used to obtain optical constants of the nanolaminates. In order to extract optical constants, we used Bruggeman effective medium (EM) approximation.¹¹ Al_2O_3 layers in nanolaminates were described using the Cauchy dispersion function,¹¹ and TiO_2 layers were characterized using one Cody–Lorentz oscillator.³³ During regression analysis the thickness of the nanolaminates was obtained fixing initial optical constants from the Woollam database in spectral range from 400 to 1000 nm. After that, Cauchy parameters A and B and Cody–Lorentz parameters were free fitting values in spectral range from 300 to 1000 nm. During these optical constants obtaining step thickness of the layers was fixed. The average amount of Al_2O_3 in nanolaminates estimated using Bruggeman effective medium approach was 67% of total volume and not depended on the number of BL. Refractive indices and extinction coefficient of the TiO_2 (a) and Al_2O_3 (b) nanolayers in nanolaminates are plotted in Figure 6 and Figure S4. All Al_2O_3 layers were transparent in all spectral range,¹¹ and the refractive index real part decreased with increased bilayer number. The obtained optical constants of Al_2O_3 were close to those reported by other authors in ref 11 and TiO_2 optical constants close to values obtained by Suchodolskis et al.³⁴ TiO_2 optical constants n and k decreased and blue-shifted with increasing number of BL. The observed phenomenon is related to improvement of crystalline structure²⁹ and increases of the packing density as described in ref 35. The obtained refractive index values were in the same range/or insignificantly higher than the same values reported by Triani et al.³⁶ It was reported that the refractive index value of TiO_2 nanolayer in $\text{Al}_2\text{O}_3/\text{TiO}_2$ nanolaminates increased and saturated when TiO_2 monolayer thickness exceeded 25 nm. It was explained by the nucleation and film growth.³⁷ However, at the present work, the saturation of

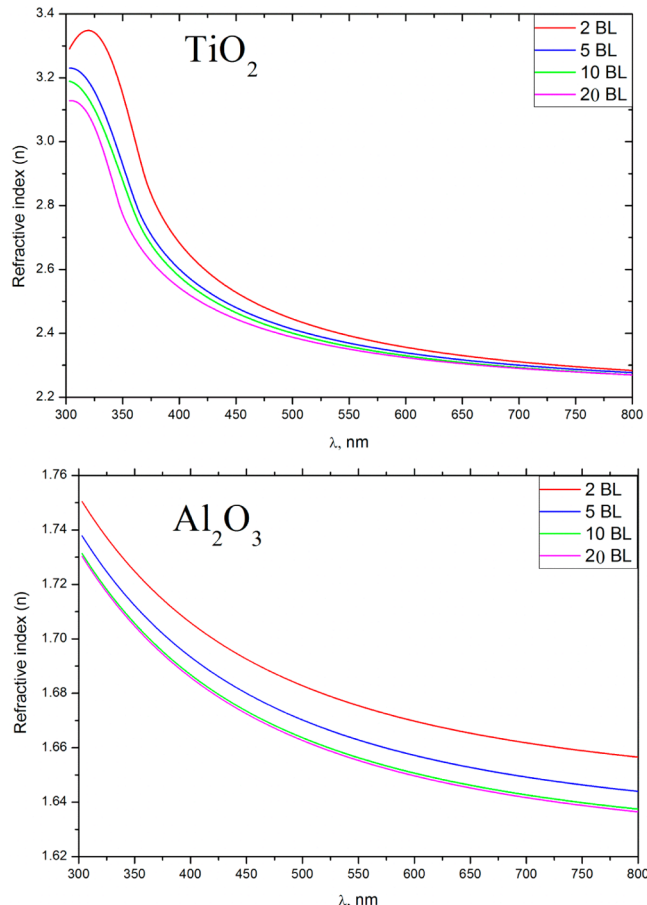


Figure 6. Average refractive indices of TiO_2 and Al_2O_3 nanolayers in $\text{TiO}_2\text{-Al}_2\text{O}_3$ nanolaminates.

refractive indices was not observed (see Table 2). It points to different nucleation rate and the layer structure, which is in good agreement with XRD and TEM measurements.

The PL spectra of nanolaminates and pure TiO_2 nanolayer (100 nm) were measured in the region of light wavelength from 400 to 700 nm (Figure 7). Two main PL peaks for the single TiO_2 nanolayer were detected at about 2.9 eV (430 nm) and 2.75 eV (450 nm), corresponding to the self-trapped excitons (STE)

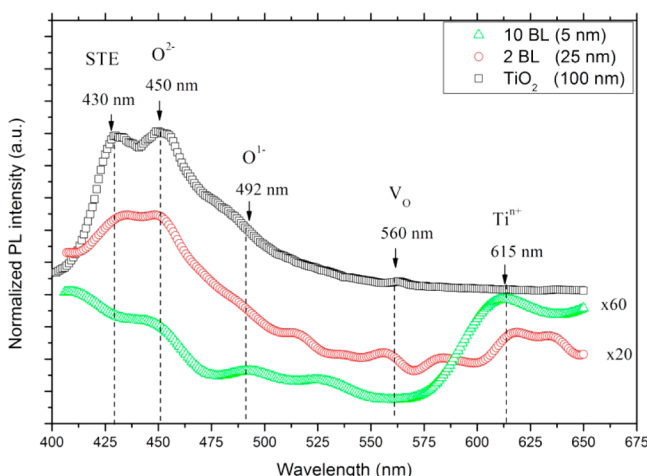


Figure 7. PL spectra of the TiO_2 layer and $\text{TiO}_2\text{/Al}_2\text{O}_3$ nanolaminates with differing numbers of BL.

localized on the TiO_6 octahedral and to oxygen vacancies with two electrons, respectively.^{29,38} There are also some weak peaks at 2.52 eV (492 nm) and 2.21 eV (560 nm) corresponding to oxygen vacancies with one electron and to the trap level related to oxygen vacancies on the surface (V_o). For nanolaminates samples, one can notice that a peak at about 2 eV (615 nm) appears. This peak, as was shown in our previous work, originates from the surface states.²⁹ These states are probably related to some surface unsaturated atoms of titanium (Ti^{4+} , Ti^{3+} , and Ti^{2+}).²⁵

From PL spectra, one can notice that two main competing recombination mechanisms (volume and surface recombination) take place. The surface recombination mechanism begins to prevail for 10 and 20 BL samples. Therefore, we can conclude that the high amount of surface defects is concentrated at the $\text{TiO}_2\text{-Al}_2\text{O}_3$ interface for these samples.

Mechanical Parameters. Hardness measurements were computed for penetration values above 10 nm; partial unloading curves were used to extract hardness and Young's modulus values at different depths. Collected values are presented in the shape of histograms, shown in Figure 8. Histograms were fitted with the kernel density estimation function.³⁹ In the case of the 2 BL sample (Figure 8a) the Young's modulus distribution shows two separate components, while the hardness shows three components. Even though the associated error overlaps, the frequency of the observed events correlates with previously reported mechanical measurements of ${}^{40}\text{TiO}_2$ and ${}^{41}\text{Al}_2\text{O}_3$ and tests performed on 75 nm single TiO_2 ($\text{Er} = 136 \pm 5$ GPa and $\text{Hr} = 7.6 \pm 0.4$) and Al_2O_3 ($\text{Er} = 143 \pm 8$ GPa and $\text{Hr} = 8.8 \pm 0.7$) films deposited by ALD in this work as control samples. However, in the case of nanolaminates, both materials show an elastic modulus of 140 ± 8 GPa, and the 157 ± 5 GPa peak is attributed to the interface between layers. The appearance of the third event, on the hardness histogram, is also attributed to the interface between layers, arousing by the influence of the substrate and bottom layers, acting as pseudosubstrates of the layers being probed.⁴¹ Sample with 4 BL is shown in Figure 8b. In this sample only two contributions are observed for both Young's modulus and hardness. As in the previous case, contributions are attributed to two effects: first, the overlapping of Al_2O_3 and TiO_2 values and, second, the interface of between layers; however, the mechanical values are improved due to the higher interfacial population. Samples with 10 and 20 BL show a bigger contribution of amorphous phases, related to the lower dimensionality of the individual layers and the increment of interfacial diffusion (Figure 8c,d). Histograms for both samples show a progressive reduction between both populations, mainly attributed to the impossibility of obtaining enough sampling between layers; typically, a film will require around 15–25% of indentation profile in order to properly assess its tribological properties.⁴² However, by using the kernel function, both contributions from layers and interfaces can be observed.

To conclude, it is clear that the increment of interfaces improves the mechanical properties of 2 and 4 BL samples due to the large crystallinity of the films. However, for 10 and 20 BL, the mechanical properties are reduced considerably due to the loss of crystallinity of each layer, which are composed of small nanocrystals, thus allowing large interdiffusion of atoms at the interfaces. Therefore, mechanical properties resemble those from amorphous films and the crystallites below the nanometer scale.

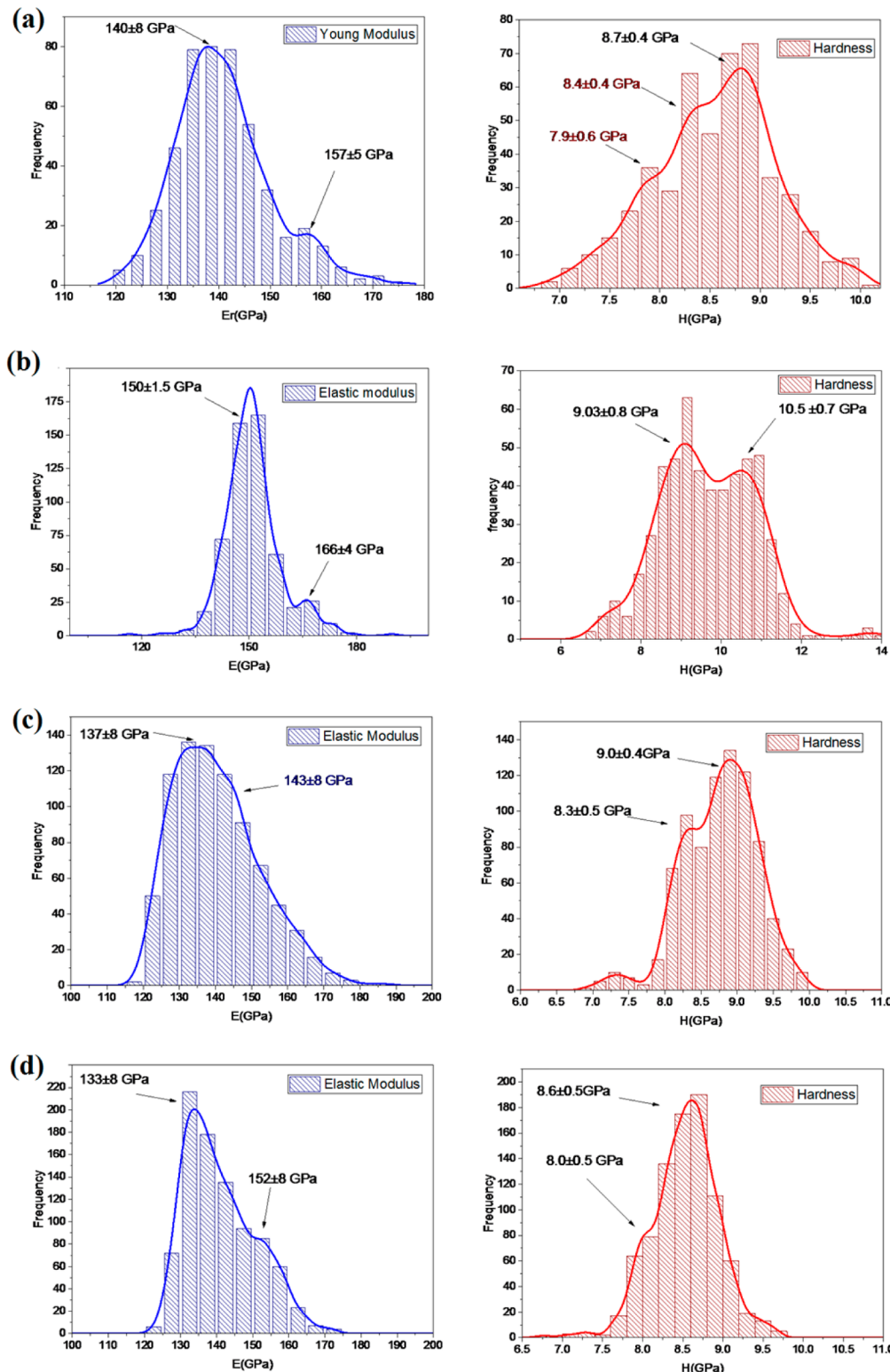


Figure 8. Histograms showing the distribution of Young's modulus (blue) and hardness (red) for samples (a) 2 BL, (b) 5 BL, (c) 10 BL, and (d) 20 BL.

4. CONCLUSIONS

In summary, $\text{Al}_2\text{O}_3/\text{TiO}_2$ nanolaminates were fabricated using atomic layer deposition. The morphology, chemical composition, and optical and mechanical properties of $\text{Al}_2\text{O}_3/\text{TiO}_2$ nanolaminates were established, and the main structural, optical, and mechanical parameters were calculated. It was shown that optical and mechanical properties of $\text{Al}_2\text{O}_3/\text{TiO}_2$ nanolaminates

are tailored by their structural parameters. The mechanism of the correlation between mechanical (Young's modulus and hardness) and optical (refractive index, band gap energy, photoluminescence) parameters was discussed. It was shown that there is an interdiffusion layer at the $\text{Al}_2\text{O}_3-\text{TiO}_2$ interface which plays a crucial role in explaining mechanical and optical properties of $\text{Al}_2\text{O}_3/\text{TiO}_2$ nanolaminates. The results obtained are very

promising for the improved use of $\text{Al}_2\text{O}_3/\text{TiO}_2$ nanolaminates in various applications where it is important to tune and control their optical and mechanical properties.

■ ASSOCIATED CONTENT

§ Supporting Information

The Supporting Information is available free of charge on the ACS Publications website at DOI: [10.1021/acs.jpcc.5b06745](https://doi.org/10.1021/acs.jpcc.5b06745).

Cross-sectional TEM images and EDX mapping analysis, Raman spectrum, and extinction coefficient of TiO_2 layers ([PDF](#))

■ AUTHOR INFORMATION

Corresponding Author

*E-mail: yatsunskiy@gmail.com (I.I.).

Notes

The authors declare no competing financial interest.

■ ACKNOWLEDGMENTS

Financial support from the National Centre for Research and Development under research grant “Nanomaterials and their application to biomedicine”, contract PBS1/A9/13/2012, is gratefully acknowledged.

■ REFERENCES

- Mikhelashvili, V.; Eisenstein, G. Composition, Surface Morphology and Electrical Characteristics of $\text{Al}_2\text{O}_3\text{-TiO}_2$ Nanolaminates and Al/TiO Films on Silicon. *Thin Solid Films* **2006**, *515*, 346.
- Lee, G.; Lai, B.; Phatak, C.; Katiyar, R. S.; Auciello, O. Interface-controlled High Dielectric Constant $\text{Al}_2\text{O}_3/\text{TiO}_x$ Nanolaminates with Low Loss and Low Leakage Current Density for New Generation Nanodevices. *J. Appl. Phys.* **2013**, *114*, 027001.
- Cho, M. H.; Roh, Y. S.; Whang, C. N.; Jeong, K. Dielectric Characteristics of $\text{Al}_2\text{O}_3 - \text{HfO}_2$ Nanolaminates on Si 100. *Appl. Phys. Lett.* **2002**, *81*, 1071–1073.
- Kim, B.; Im, J.; Lee, B. Y.; Sung, M. G.; Heo, K.; Bak, J. H.; Park, Y. D.; Hong, S. Carbon Nanotubes – Metal Nanolamine for Enhanced Strength and Electrical Conductivity. *Carbon* **2011**, *49*, 2549–2554.
- Chawla, N.; Singh, D. R. P.; Shen, Y. L.; Tang, G.; Chawla, K. K. Indentation Mechanics and Fracture Behavior of Metal/Ceramic Nanolamine Composites. *J. Mater. Sci.* **2008**, *43*, 4383–4390.
- Tripp, M. K.; Stampfer, C.; Miller, D. C.; Helbling, T.; Herrmann, C. F.; Hierold, C.; Gall, K.; George, S. M.; Bright, V. M. The Mechanical Properties of Atomic Layer Deposited Alumina for Use in Micro- and Nano-electromechanical Systems. *Sens. Actuators, A* **2006**, *130*–*131*, 419–429.
- Lee, G.; Lai, B.; Phatak, C.; Katiyar, R. S.; Auciello, O. Effects of the Interfacial Layer on Electrical Characteristics of $\text{Al}_2\text{O}_3/\text{TiO}_2/\text{Al}_2\text{O}_3$ Thin Films for Gate Dielectrics. *Appl. Surf. Sci.* **2012**, *258*, 3089–3093.
- Cheun, H.; Fuentes-Hernandez, C.; Shim, J.; Fang, Y.; Cai, Y.; Li, H.; Sigdel, A. K.; Meyer, J.; Maibach, J.; Dindar, A.; Zhou, Y.; Berry, J. J.; Bredas, J.; Kahn, A.; Sandhage, K. H.; Kippelen, B. Oriented Growth of $\text{Al}_2\text{O}_3:\text{ZnO}$ Nanolaminates for Use as Electron-Selective Electrodes in Inverted Polymer Solar Cells. *Adv. Funct. Mater.* **2012**, *22*, 1531–1538.
- Park, S. H. K.; Hwang, S.; Jeong, Y.; Chu, H. Y.; Cho, K. I. Transparent ZnO-TFT Arrays Fabricated by Atomic Layer Deposition. *Electrochem. Solid-State Lett.* **2008**, *11*, H10.
- Chaaya, A. A.; Viter, R.; Balevičiute, I.; Bechelany, M.; Ramanavicius, A.; Ertas, D.; Smyntyna, V.; Miele, P. Optical and Structural Properties of $\text{Al}_2\text{O}_3/\text{ZnO}$ Nanolaminates Deposited by ALD Method. *Physica status solidi (c)* **2014**, *11*, 1505–1508.
- Chaaya, A. A.; Viter, R.; Balevičiute, I.; Bechelany, M.; Ramanavicius, A.; Gertnere, Z.; Ertas, D.; Smyntyna, V.; Miele, P. Tuning Optical Properties of $\text{Al}_2\text{O}_3\text{-ZnO}$ Nanolaminates Synthesized by Atomic Layer Deposition. *J. Phys. Chem. C* **2014**, *118*, 3811–3819.
- Giannakopoulou, T.; Todorova, N.; Giannouri, M.; Yu, J.; Trapalis, C. Optical and Photocatalytic Properties of Composite TiO_2/ZnO Thin Films. *Catal. Today* **2014**, *230*, 174–180.
- Wang, W. C.; Tsai, M. C.; Yang, J.; Hsu, C.; Chen, M. J. Efficiency Enhancement of Nanotextured Black Silicon Solar Cells Using $\text{Al}_2\text{O}_3/\text{TiO}_2$ Dual-Layer Passivation Stack Prepared by Atomic Layer Deposition. *ACS Appl. Mater. Interfaces* **2015**, *7*, 10228–10237.
- Han, D. S.; Choi, D. K.; Park, J. V. $\text{Al}_2\text{O}_3/\text{TiO}_2$ Multilayer Thin Films Grown by Plasma Enhanced Atomic Layer Deposition for Organic Light-Emitting Diode Passivation. *Thin Solid Films* **2014**, *552*, 155–158.
- Kim, L. H.; Kim, K.; Park, S.; Jeong, Y. J.; Kim, H.; Chung, D. S.; Kim, S. H.; Park, C. E. $\text{Al}_2\text{O}_3/\text{TiO}_2$ Nanolaminate Thin Film Encapsulation for Organic Thin Film Transistors via Plasma-Enhanced Atomic Layer Deposition. *ACS Appl. Mater. Interfaces* **2014**, *6*, 6731–6738.
- Zhang, G. Z.; Wu, H.; Chen, C.; Wang, T.; Wang, P. Y.; Mai, L. Q.; Yue, J.; Liu, C. Transparent Capacitors Based on Nanolaminate $\text{Al}_2\text{O}_3/\text{TiO}_2/\text{Al}_2\text{O}_3$ with H_2O and O_3 as Oxidizers. *Appl. Phys. Lett.* **2014**, *104*, 163503.
- Mukherjee, C.; Das, T.; Mahata, C.; Maiti, C. K.; Chia, C. K.; Chiam, S. Y.; Chi, D. Z.; Dalapati, G. K. Interface Properties of Atomic Layer Deposited $\text{TiO}_2/\text{Al}_2\text{O}_3$ Films on $\text{In}_{0.53}\text{Ga}_{0.47}\text{As}/\text{InP}$ Substrates. *ACS Appl. Mater. Interfaces* **2014**, *6*, 3263–3274.
- Suh, D.; Choi, D. Y.; Weber, K. J. $\text{Al}_2\text{O}_3/\text{TiO}_2$ Stack Layers for Effective Surface Passivation of Crystalline Silicon. *J. Appl. Phys.* **2013**, *114*, 154107.
- Spinelli, P.; Macco, B.; Verschuuren, M. A.; Kessels, W. M. M.; Polman, A. $\text{Al}_2\text{O}_3/\text{TiO}_2$ Nano-pattern Antireflection Coating with Ultralow Surface Recombination. *Appl. Phys. Lett.* **2013**, *102*, 233902.
- Song, X.; Takoudis, C. G. Cyclic chemical vapor deposited $\text{TiO}_2/\text{Al}_2\text{O}_3$ films using trimethyl aluminum, tetrakis(diethylamino)titanium and O_2 . *J. Electrochem. Soc.* **2007**, *154*, G177–182.
- Rowlette, P. C.; Wolden, C. A. Pulsed plasma-enhanced chemical vapor deposition of $\text{Al}_2\text{O}_3\text{-TiO}_2$ nanolaminates. *Thin Solid Films* **2010**, *518*, 3337–3341.
- Walke, P.; Bouregba, R.; Lefevre, A.; Parat, G.; Lallemand, F.; Voiron, F.; Mercey, B.; Lüders, U. Giant dielectric constant in $\text{TiO}_2/\text{Al}_2\text{O}_3$ nanolaminates grown on doped silicon substrate by pulsed laser deposition. *J. Appl. Phys.* **2014**, *115*, 094103.
- Iatsunskyi, I.; Kempinski, M.; Jancelewicz, M.; Zalesski, K.; Jurga, S.; Smyntyna, V. Structural and XPS Characterization of ALD Al_2O_3 Coated Porous Silicon. *Vacuum* **2015**, *113*, 52–58.
- Iatsunskyi, I.; Jancelewicz, M.; Nowaczyk, G.; Kempinski, M.; Peplińska, B.; Jarek, M.; Zalesski, K.; Jurga, S.; Smyntyna, V. Atomic Layer Deposition TiO_2 Coated Porous Silicon Surface: Structural Characterization and Morphological Features. *Thin Solid Films* **2015**, *589*, 303–308.
- Iatsunskyi, I.; Kempinski, M.; Nowaczyk, G.; Jancelewicz, M.; Pavlenko, M.; Zalesski, K.; Jurga, S. Structural and XPS Studies of PSi/ TiO_2 Nanocomposites Prepared by ALD and Ag-assisted Chemical Etching. *Appl. Surf. Sci.* **2015**, *347*, 777–783.
- Oliver, W.; Pharr, G. An Improved Technique for Determining Hardness and Elastic Modulus Using Load and Displacement Sensing Indentation Experiments. *J. Mater. Res.* **1992**, *7*, 1564–1583.
- Sintonen, S.; Ali, S.; Ylivaara, O. M. E.; Puurunen, R. L.; Lipsanen, H. X-ray Reflectivity Characterization of Atomic Layer Deposition $\text{Al}_2\text{O}_3/\text{TiO}_2$ Nanolaminates with Ultrathin Bilayers. *J. Vac. Sci. Technol., A* **2014**, *32*, 01A111.
- Aarik, J.; Aidla, A.; Uustare, T.; Sammelselg, V. Morphology and Structure of TiO_2 Thin Films Grown by Atomic Layer Deposition. *J. Cryst. Growth* **1995**, *148*, 268–275.
- Iatsunskyi, I.; Pavlenko, M.; Viter, R.; Jancelewicz, M.; Nowaczyk, G.; Balevičiute, I.; Zalesski, K.; Jurga, S.; Ramanavicius, A.; Smyntyna, V. Tailoring the Structural, Optical, and Photoluminescence Properties of Porous Silicon/ TiO_2 Nanostructures. *J. Phys. Chem. C* **2015**, *119*, 7164–7171.

- (30) Lin, S. S.; Wu, D. K. The Properties of Al-doped TiO₂ Nanoceramic Films Deposited by Simultaneous rf and dc Magnetron Sputtering. *Ceram. Int.* **2010**, *36*, 87–91.
- (31) Choudhury, B.; Choudhury, A. Oxygen Defect Dependent Variation of Band Gap, Urbach Energy and Luminescence Property of Anatase, Anatase–Rutile Mixed Phase and of Rutile Phases of TiO₂ Nanoparticles. *Phys. E* **2014**, *56*, 364–371.
- (32) Tang, H.; Levy, F.; Berger, H.; Schmid, P. E. Urbach Tail of Anatase TiO₂. *Phys. Rev. B: Condens. Matter Mater. Phys.* **1995**, *52*, 7771–7774.
- (33) Horprathum, M.; Kaewkhai, J.; Eiamchai, P.; Chindaodom, P.; Limsuwan, P. Investigation of Inhomogeneity of TiO₂ Thin Films Using Spectroscopic Ellipsometry. *Journal of Physics: Conference Series* **2013**, *417*, 012007.
- (34) Suchodolskis, A.; Reza, A.; Bukauskas, V.; Mironas, A.; Setkus, A.; Simkiene, I. Optical Study of Ultrathin TiO₂ Films for Photovoltaic and Gas Sensing Applications. *Mater. Sci.* **2014**, *20*, 150–152.
- (35) Wang, X.; Wu, G.; Zhou, B.; Shen, J. Optical Constants of Crystallized TiO₂ Coatings Prepared by Sol-Gel Process. *Materials* **2013**, *6*, 2819–2830.
- (36) Triani, G.; Evans, P. J.; Mitchell, D. R. G.; Attard, D. J.; Finnie, K. S.; James, M.; Hanley, T.; Latella, B.; Prince, K. E.; Bartlett, J.; Michael, L.; Fulton, J.; Kruschwitz, D. T. Atomic Layer Deposition of TiO₂/Al₂O₃ Films For Optical Applications, Advances in Thin-Film Coatings for Optical Applications II. *Proc. SPIE* **2005**, *5870*, 587009.
- (37) Triani, G.; Campbell, J. A.; Evans, P. J.; Davis, J.; Latella, B. A.; Burford, R. P. Low Temperature Atomic Layer Deposition of Titania Thin Films. *Thin Solid Films* **2010**, *518*, 3182–3189.
- (38) Kernazhitsky, L.; Shymanovska, V.; Gavrilko, T.; Naumov, V.; Fedorenko, L.; Kshnyakin, V.; Baran, J. Room Temperature Photoluminescence of Anatase and Rutile TiO₂ Powders. *J. Lumin.* **2014**, *146*, 199–204.
- (39) Wand, M. P.; Jones, M. C. *Kernel Smoothing*; Chapman & Hall/CRC Monographs on Statistics & Applied Probability (60); Chapman & Hall: Boca Raton, FL, 1994.
- (40) Jung, H.; Park, C.; Lee, J.; Park, Y. S. Tribological and Electrical Properties of TiO₂ Thin Films for Polymer Insulator as the Dielectric Coating of Electric Railroad. *Mater. Res. Bull.* **2014**, *58*, 44–48.
- (41) Tripp, M. K.; Stampfer, C.; Miller, D. C.; Helbling, T.; Herrmann, C. F.; Hierold, C.; Gall, K.; George, S. M.; Bright, V. M. The Mechanical Properties of Atomic Layer Deposited Alumina for Use in Micro- and Nano-electromechanical Systems. *Sens. Actuators, A* **2006**, *130–131*, 419–429.
- (42) Korsunsky, A. M.; McGurk, M. R.; Bull, S. J.; Page, T. F. On the Hardness of Coated Systems. *Surf. Coat. Technol.* **1998**, *99*, 171–183.